Mesoporous Ta Oxide. 2. Improvement of the Synthetic Method and Observation of Mesostructure Formation

Junko N. Kondo, Yoshiko Takahara, Daling Lu,† and Kazunari Domen*,†

Chemical Resources Laboratory, Tokyo Institute of Technology, 4259 Nagatsuta, Midori-ku, Yokohama 226-8503, Japan

Received October 31, 2000. Revised Manuscript Received February 9, 2001

The ligand-assisted templating method for the production of mesoporous Ta_2O_5 was improved by the removal of noncoordinating alkylamine surfactant before aging. The improved method increased the uniformity of the porous structure and the particle size. The immediate precipitation after the hydrolysis of the alkylamine-coordinated $Ta(OEt)_5$ allowed the detailed observation of the powder particles at each synthesis step by XRD, N_2 adsorption isotherms, SEM, and TEM. TEM and XRD observations found that micelle rods already existed in particles formed soon after hydrolysis. Therefore, micelle rods were suggested to be formed even in the absence of water. Final aging at 453 K encouraged the arrangement of the mesopores in a wormhole-like structure, which was evidenced by the type H2 hysteresis loop of the desorption branch of N_2 adsorption−desorption isotherms in addition to TEM images.

Introduction

Various mesoporous transition metal oxides have been successfully synthesized using various types of surfactants.[1−14] Among them, we have been interested in photocatalytically active TiO_2, Ta_2O_5, and Nb_2O_5, whose synthetic methods are reported by Ying et al.[1,8−10] Mesoporous Ta_2O_5 and Nb_2O_5 are formed by the so-called ligand-assisted templating method, where $M(OEt)_5$ (M = Nb and Ta) is first covalently bonded to alkylamine to form a complete hexavalent configuration, $M(OEt)_5(C_nH_{2n+1}NH_2)$, where M denotes Nb or Ta. Then, water is added to produce precipitate immediately. The precipitate is settled in water and is hydrothermally treated to proceed dehydration and condensation. One of the unique features of this method is the immediate formation of precipitate, differently from other sol−gel systems. However, the details of the aging process of this method are not yet clear.

Recently, photocatalytic activity for overall water decomposition on Ta-containing mixed oxides has been reported.[15−20] Therefore, we synthesized mesoporous Ta_2O_5 and studied the photocatalytic behavior for overall water splitting.[21] While its photocatalytic capability was attractive, problems arose on the poor reproducibility of the property of the product; neither the same BET surface area nor the same pore size distribution was always obtained even through the same synthesis procedure. Another problem was the poorly ordered mesoporous structure. XRD patterns and pore size distributions obtained from the adsorption branch of N_2 adsorption isotherms were not as clear as those of MCM-41. The poor thermal stability was also one of the disadvantages for the activation of mesoporous Ta_2O_5 as a photocatalyst.[21] Therefore, we optimized the synthetic approach for mesoporous Ta_2O_5. As a result, fine particles with better mesoporous structure were obtained. In this study the states of the sample at each step during the synthesis were examined by X-ray diffraction (XRD), N_2 adsorption isotherms, scanning electron microscopy (SEM), and transmission electron microscopy (TEM).

Experimental Section

Synthesis. Mesoporous Ta_2O_5 was synthesized following the ligand-assisted templating method, the procedure reported by

* To whom correspondence should be addressed. Fax: +81-45-924-5282. Tel.: +81-45-924-5238. E-mail: kdomen@res.titech.ac.jp.

† Core Research for Evolutional Science and Technology (CREST), Japan Science and Technology (JST).

(1) Ying, J. Y.; Mehnert, C. P.; Wong, M. S. *Angew. Chem., Int. Ed.* **1999**, *38*, 56.
(2) Luca, V.; Maclachlan, D. J.; Hook, J. M.; Withers, R. *Chem. Mater.* **1995**, *7*, 220.
(3) Antonelli, D. M.; Ying, J. Y. *Angew. Chem., Int. Ed. Engl.* **1995**, *34*, 2014.
(4) Fujii, H.; Ohtaki, M.; Eguchi, K. *J. Am. Chem. Soc.* **1998**, *120*, 6832.
(5) Pacheco, G.; Zhao, E.; Garcia, A.; Sklyarov, A.; Fropiat, J. J. *Chem. Commun.* **1999**, 491.
(6) Wong, M. S.; Ying, J. Y. *Chem. Mater.* **1998**, *10*, 2067.
(7) Ciesla, U.; Fröba, M.; Stucky, G. D.; Schüth, F. *Chem. Mater.* **1999**, *11*, 227.
(8) Antonelli, D. M.; Ying, J. Y. *Chem. Mater.* **1996**, *58*, 874.
(9) Antonelli, D. M.; Ying, J. Y. *Angew. Chem., Int. Ed. Engl.* **1996**, *35*, 426.
(10) Antonelli, D. M.; Nakahira, A.; Ying, J. Y. *Inorg. Chem.* **1996**, *35*, 3126.
(11) Tian, Z. R.; Tong, W.; Wang, J. Y.; Duan, N. G.; Krishnan, V. V.; Suib, S. L. *Science* **1997**, *276*, 926.
(12) Chen, F.; Liu, M. *Chem. Commun.* **1999**, 1829.
(13) Yang, P.; Zhao, D.; Margolese, D. I.; Chmelka, B. F.; Stucky, G. D. *Nature* **1998**, *396*, 152.
(14) Yang, P.; Zhao, D.; Margolese, D. I.; Chmelka, B. F.; Stucky, G. D. *Chem. Mater.* **1999**, *11*, 2813.
(15) Kudo, A.; Kato, H. *Chem. Lett.* **1997**, 867.
(16) Kato, H.; Kudo, A. *Chem. Phys. Lett.* **1999**, 1027.
(17) Ishihara, T.; Nishiguchi, H.; Fukamachi, K.; Takita, Y. *J. Phys. Chem. B* **1999**, *103*, 1.
(18) Kato, H.; Kudo, A. *Catal. Lett.* **1999**, *58*, 183.
(19) Kato, H.; Kudo, A. *Chem. Lett.* **1999**, 1027.
(20) Kudo, A.; Kato, H.; Nakagawa, S. *J. Phys. Chem. B* **2000**, *104*, 571.
(21) Takahara, Y.; Kondo, J. N.; Takata, T.; Lu, D.; Domen, K. *Chem. Mater.* **2001**, *13*, 1194.

10.1021/cm000865b CCC: $20.00
Published on Web 04/16/2001

Antonelli and Ying.[8] Octadecylamine (Kanto Chemicals, 1.65 g, 6.15 mmol) was mixed in $Ta(OEt)_5$ (Aldrich or Kojundo Chemical Laboratory, 5.0 g, 12.30 mmol) under an Ar gas atmosphere and warmed to 323 K for 10−30 min until octadecylamine was dissolved completely; that is, a homogeneous clear liquid was obtained. To these organic metal complexes was added deionized water (Seiki Medicine Kougyou) through a spray with stirring. Hydrolyzation occurred immediately to form fine white particles. The deionized water was poured gradually up to 25 mL. The precipitation was kept in the supernatant at room temperature for 24−48 h and transferred to a Teflon beaker for aging at 353 K for 1 day, 373 K for 1 day, and 453 K for 7 days, successively. The product was collected by suction filtration and washed with the deionized water, ethanol (Kanto Chemicals), and diethyl ether (Kanto Chemicals). The powder was then dried at 373 K for 12 h in the atmosphere to obtain the precursor.

The precursor (1 g) was suspended in dimethoxyethane at 195 K under an Ar atmosphere, treated with trifluoromethane sulfonic acid (Aldrich, 0.113 mL, 1.28 mmol), and kept for 1 h at the same temperature with stirring. The suspension was warmed to the ambient temperature and stirred for another 2 h. The powder was collected by suction filtration, washed with 2-propanol (Kanto Chemicals), and transferred to a beaker for washing in 2-propanol at room temperature for 1 day. The powder was collected by suction filtration with washing by deionized water, ethanol, and diethyl ether, respectively, and then dried in evacuation at 373 K within 12 h.

Characterization. Powder X-ray diffraction patterns (XRD) of the products were obtained on a Rigaku Rint 2000 diffractometer using Cu Kα radiation (40 kV, 40 mA) at a 0.02 step size and 1-s step time over the range $1.5° < 2\theta < 15°$. A background was subtracted in the XRD patterns shown in the present study. N_2 adsorption−desorption isotherms at 77 K were measured using a Micrometrics Coulter Omnisorp 100CX system. Samples were normally prepared for N_2 adsorption measurement by degassing at 373 K under vacuum until a final pressure of 1×10^{-5} Torr was reached. BET surface areas were estimated over a relative pressure (P/P_0) ranging from 0.05 to 0.30. Pore size distributions were obtained from the analysis of the adsorption branch of the isotherms using the BJH (Barrett−Joyner−Halenda) method. Images of SEM and TEM were observed on a Hitachi S-4700 FE-SEM and on a JEOL 2010F electron microscope operated at 200 keV, respectively. The samples for TEM observation were prepared by dipping a drop of mesoporous Ta_2O_5 powder in 2-propanol on the copper grid covered with carbon film.

Results and Discussion

Improvement of the Mesoporous Structure of Ta_2O_5. Although the molar ratio of $Ta(OEt)_5$ to octadecylamine was adjusted to 2:1 according to the synthetic condition reported in the reference,[8] we considered the presence and the effect of noncoordinating surfactant molecules on the aging process and attempted to wash the precipitate product before aging. The precipitate formed after hydrolysis of $Ta(OEt)_5$ was once collected for washing by water, ethanol (twice), and water again. Hydrothermal treatment was then conducted with another 25 mL of water at room temperature for 1 day, 353 K for 1 day, 373 K for 1 day, and 453 K for 7 days. Figure 1A compares the adsorption branch of N_2 isotherms of the mesoporous Ta_2O_5 samples produced by the conventional method without washing before aging (a) and by the present method (b), both after aging and surfactant removal. The type IV pattern of the isotherms identical to the mesoporous materials was obviously improved by washing the precipitate product before aging, although the BET surface area was only slightly increased from 405 to 431 $m^2\ g^{-1}$. The pore size distribution of the sample (a) and (b) in Figure 1A is also compared in Figure 1B. The mesoporous Ta_2O_5 produced without washing indicated only a poor pore size distribution (a), while those formed from the washed precipitates showed sharp pore size distributions (b). Assuming that noncoordinating amine surfactant molecules to $Ta(OEt)_5$ were participating in micelle formation, their presence would hinder the homogeneous polymerization of the inorganic part as well as the formation of uniform micelle rods. The elimination of the free surfactant might result in a homogeneous environment of Ta species, that is, homogeneous formation of the oxide phase.

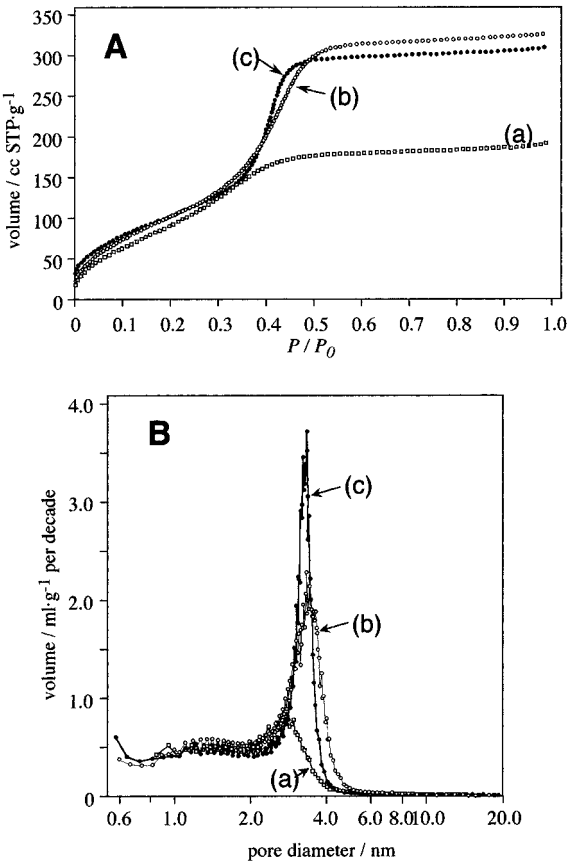

Figure 1. Comparison of N_2 adsorption isotherms (A) and pore size distributions (B) on mesoporous Ta_2O_5 synthesized by the conventional method (a) and by improved methods (b and c). Water was added through a beaker at once in the case of (a) and (b), while a spray was used for the sample (c).

For the production of both samples (a) and (b) water was added instantaneously from a beaker to hydrolyze $Ta(OEt)_5$. We next attempted to add water through a spray. Fine white particles were obtained when the spray addition was employed. As shown in Figure 1A-(c), an improved type IV isotherm pattern was observed by N_2 adsorption isotherms. By comparing the pore size distributions of (b) and (c) in Figure 1B, the spray addition of water was confirmed to be preferable to the conventional method. SEM images of samples prepared by the conventional (Figure 2A) and improved (Figure 2B) methods both aged at 453 K shows the morphological difference. The conventional method, where water was added instantaneously, produced larger particles in comparison with the improved method using a spray for water addition. Although the particle size distribu-

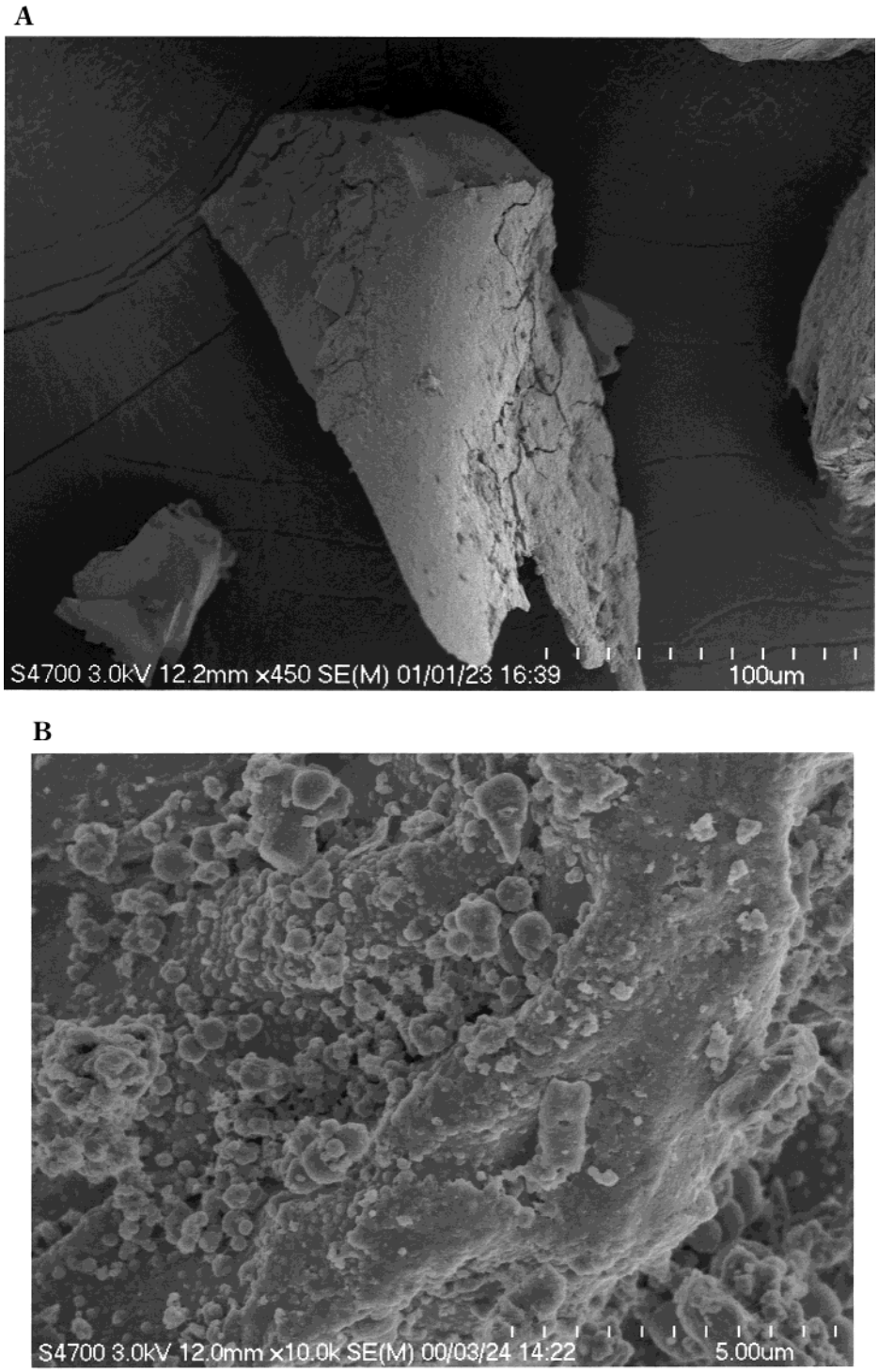

Figure 2. SEM images of mesoporous Ta_2O_5 samples prepared by the conventional (A) and the improved (B) methods, both after aging at 453 K for 7 days.

tions of both samples are in wide ranges, the dominant size was some hundreds of nanometers for the one prepared by the conventional method and several tens of nanometers for the improved method. It was also noted that the outer surface of particles in Figure 2A is rather flat, while fine spherical particles are observed in Figure 2B. In addition to the spherical particle, the improved method also produced spongelike aggregates of fine particles several nanometers in size (not shown). The improvement by the spray addition is probably responsible for the homogeneous hydrolysis around small water droplets. Thus, we optimized the condition of hydrolysis to the addition of water through a spray and the aging process to washing out the residual surfactant soon after hydrolysis previously.

The aging process and condition were then examined by XRD and N_2 adsorption isotherms. The aging was performed at 353 K for 1 day and 373 K for 1 day, followed by aging either at 423 K (Figure 3A) or 453 K (Figures 3B and 3C) for 7 days. In the case of the sample in Figure 3C, the precipitate was further aged at 473 K for 1 day. Precipitates were collected at each step of aging for XRD measurement. The upper XRD patterns in each trace (A(d), B(d) and C(e)) are attributed to the

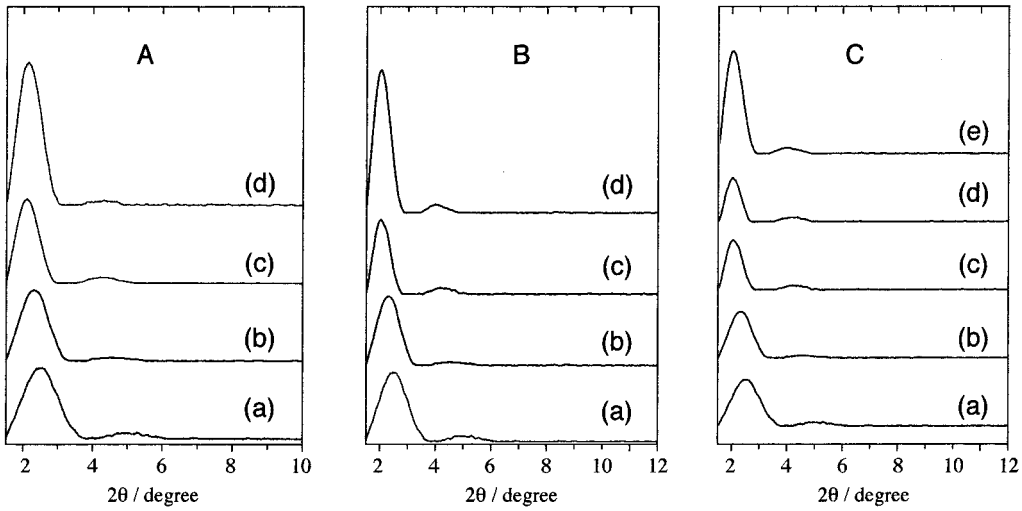

Figure 3. XRD patterns of mesoporous Ta_2O_5 samples during hydrothermal treatment. Samples were treated up to 423 K (A), 453 K (B), and 473 K (C). Patterns (a) and (b) were measured soon after hydrolysis (a) and after hydrothermal treatment at 373 K (b). A(c) and A(d) were measured after aging at 423 K and after surfactant removal. B(c) and B(d) were measured after aging at 453 K and after surfactant removal. C(c), C(d), and C(e) were measured after aging at 423 K, followed by further aging at 473 K and after surfactant removal, respectively.

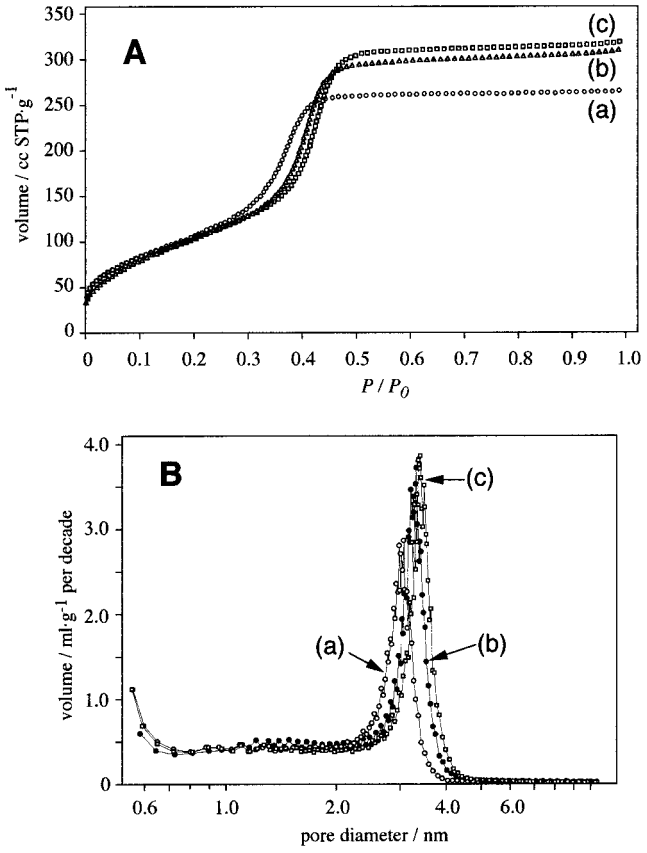

Figure 4. Comparison of N_2 adsorption isotherms (A) and pore size distributions (B) on mesoporous Ta_2O_5 synthesized by different aging conditions as described in Figure 3; see text.

mesoporous Ta_2O_5 after the surfactant removal. A broad diffraction was already observed at ca. 2.5° for the particles before aging (a), indicating that micelle rods that were homogeneous in diameter already existed in the precipitates collected soon after hydrolysis. Because (110) and (200) diffraction peaks identical to the hexagonal mesoporous structure were not observed clearly, the pore structure of the mesoporous Ta_2O_5 was not assigned to hexagonal. The intense diffraction at $2\theta <$ 3.0° shifted to a lower angle and became sharper by the proceeding hydrothermal treatment. The gradual change of micelle rods to homogeneous phase and increase in pore size (mentioned below) are implied by these results. Even at the final stage of aging, (110) and (200) diffraction peaks due to the hexagonal mesoporous structure did not become clear. Therefore, the strong diffraction at $2\theta < 3.0°$ is rather considered to be caused by an isomorphous distribution of wall and/or mesopores with similar sizes. Although XRD data of the final products are implied to be disordered mesoporous structures with homogeneous pore sizes, we tentatively refer to the intense diffraction peak as the (100) peak hereafter for simplicity. In a comparison of the XRD patterns of surfactant-removed mesoporous Ta_2O_5, (A) showed a broader (100) diffraction than (B) and (C). Therefore, it was suggested that 423 K was not a sufficiently high temperature for aging. Hydrothermal treatment at 453 and 473 K did not show a large difference in XRD results.

Table 1. Analysis of Mesoporous Ta_2O_5 Synthesized by Aging at Different Temperatures

aging temp (K)	BET surface area ($m^2\ g^{-1}$)	pore size (nm)	d(100) (nm)
423	413	3.0	4.2
453	410	3.3	4.4
473	402	3.4	4.4

N_2 adsorption isotherms were measured for template-removed samples aged at different temperatures (corresponding to A(d), B(d), and C(e) in Figure 3). Although the type IV isotherm pattern was found for all the samples as shown in Figure 4A, the type IV curve was found to be improved by increasing the aging temperature from 423 to 453 K. The pore size was found to be increased by increasing the temperature of final aging as shown in Figure 4B. The results from XRD and N_2 adsorption isotherms are summarized in Table 1. BET surface areas higher than 400 $m^2\ g^{-1}$ were obtained for all the samples, and the value of d(100) and the pore size did not show much difference for the sample aged at temperatures above 450 K. These results confirmed that the temperature higher than 450 K was necessary

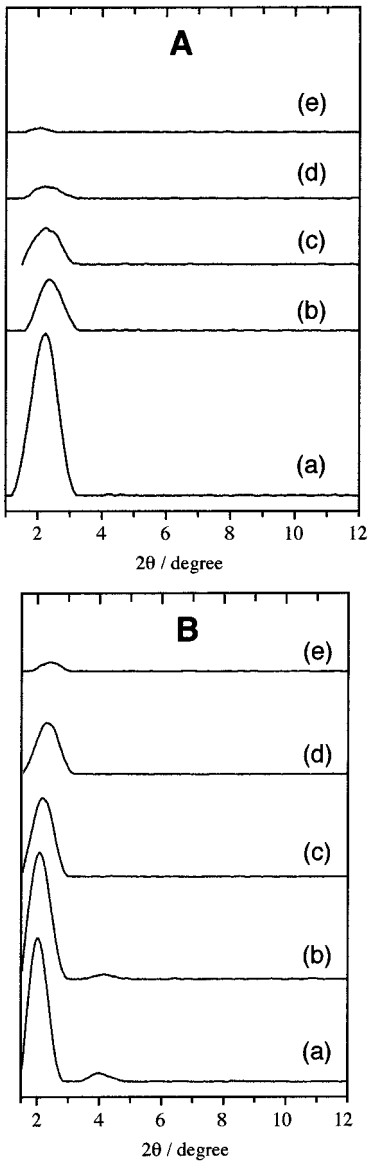

Figure 5. XRD patterns to show the thermal stability of mesoporous Ta_2O_5 samples synthesized by the conventional method (A) and by improved method (B). As-prepared samples (a) were calcined either at 473 K (b), 573 K (c), 673 K (d), or 773 K (e) in air.

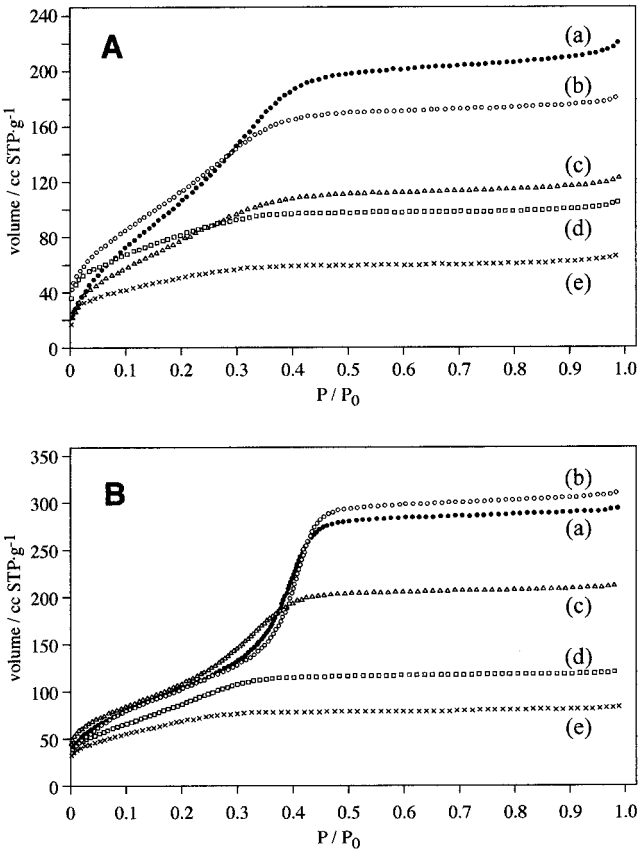

Figure 6. N_2 adsorption isotherms to show the thermal stability of mesoporous Ta_2O_5 samples synthesized by the conventional method (A) and by improved method (B). As-prepared samples (a) were calcined either at 473 K (b), 573 K (c), 673 K (d), or 773 K (e) in air.

Table 2. Change of BET Surface Area upon Calcination of Mesoporous Ta_2O_5 (m^2 g^{-1})

calcination temperature	conventional method	improved method
none	427	410
473 K	417	397
573 K	310	387
673 K	290	330
773 K	180	253

to complete aging. The increase of the *d*(001) value by 0.2 nm by increasing the aging temperature from 423 to 453 K corresponds to the increase of the repeated distance by 0.22 nm. A simultaneous increase in pore size was observed from ca. 3.0 to 3.2−3.3 nm (Figure 4B). Therefore, the wall thickness is considered to be unaffected during the aging process.

Thermal Resistibility of the Mesoporous Structure. The thermal resistibility of the mesoporous Ta_2O_5 samples synthesized by the conventional (Figures 5A and 6A) and the improved (Figures 5B and 6B) methods was compared by XRD (Figure 5) and N_2 adsorption isotherms (Figure 6). Both samples were prepared by hydrothermal treatment at 353 K for 1 day, 373 K for 1 day, and 453 K for 7 days. After the surfactant removal, the prepared samples were calcined either at 473, 573, 673, or 773 K for 1 h in air. The (100) diffraction peak of the mesoporous Ta_2O_5 prepared by the conventional method extremely decreased in intensity when calcined at 473 K and then gradually weakened with increasing the calcination temperature. On the other hand, the improved synthesizing method also increased the thermal resistibility of the mesoporous Ta_2O_5: calcination at 473 K did not so much affect the XRD pattern and about half of the intensity of the (100) diffraction still remained on the sample calcined at 673 K.

The advantage of the improved method for the thermal resistibility also appeared in the sustenance of the type IV pattern of N_2 adsorption isotherms as well as BET surface areas as compared in Figure 6 and Table 2. The type IV isotherm was not changed after calcination of the sample prepared by the present method at 473 K, while that of the sample produced by the conventional method already commenced to be destroyed after calcination at the same temperature. This result is in good agreement with the XRD patterns observed in Figure 5. Although the isotherms of both mesoporous Ta_2O_5 samples after calcination at 773 K seemed to be almost the same, the difference was seen in the BET surface area. The improved sample still

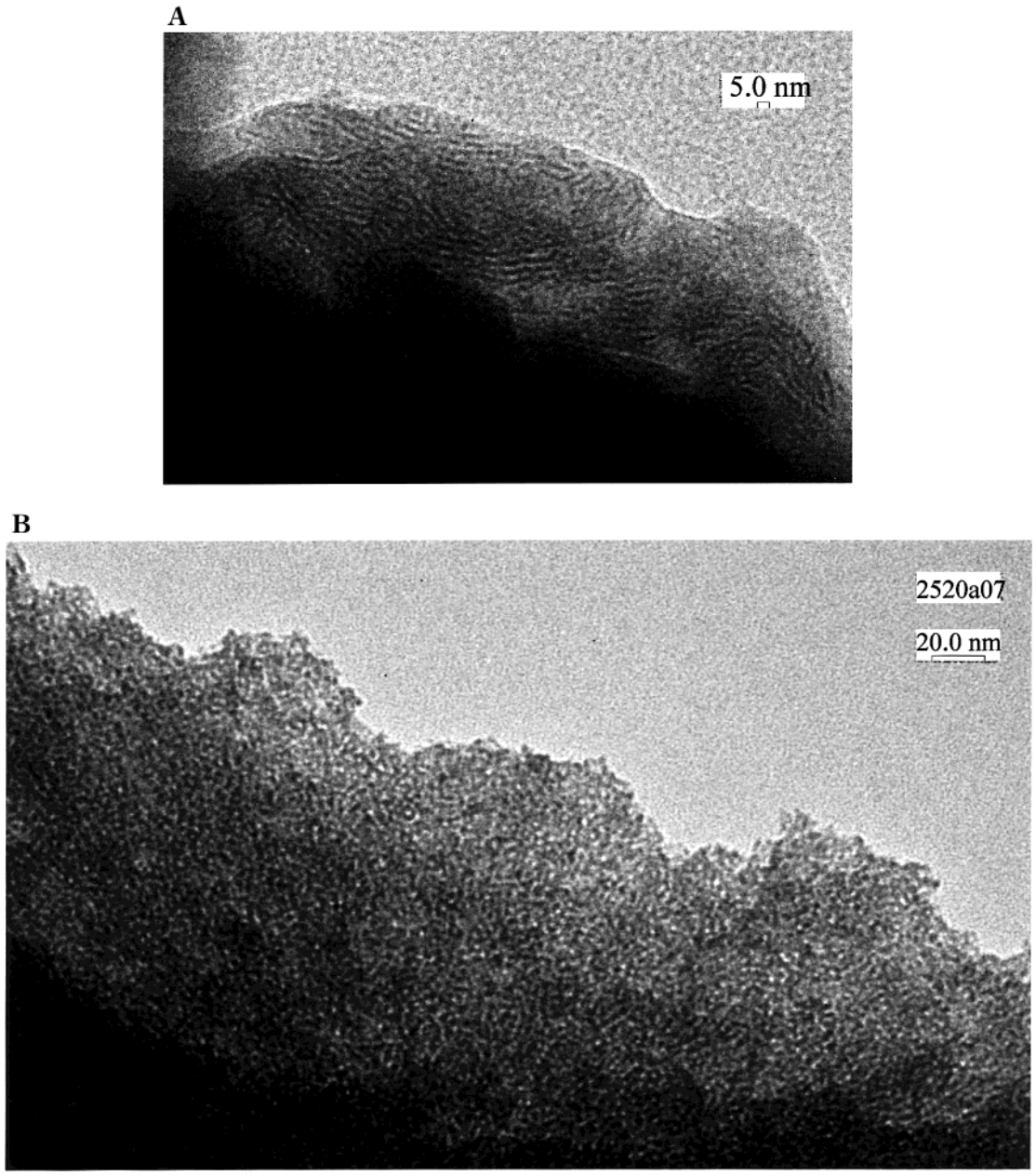

Figure 7. TEM images of mesoporous Ta_2O_5 samples soon after hydrolysis (A) and after aging at 453 K followed by further aging at 473 K (B).

possessed high surface area (253 $m^2\ g^{-1}$) even after calcination at 773 K. This corresponds to SiO_2 with more than 900 $m^2\ g^{-1}$ when one estimates the value by converting from Ta_2O_5 to Si_2O_4 unit. Therefore, the mesoporous Ta_2O_5 prepared by the improved method is expected to be practically utilized for various applications, although Ta_2O_5 consisting of the wall was confirmed to be amorphous by XRD. (An exothermal peak due to crystallization was observed only at 984 K at a heating rate of 10 $K \cdot min^{-1}$.)

TEM Observation and Arrangement of Mesopores. The formation of precipitates from the initial stage of the aging process enabled us to visually observe the samples by TEM in addition to the results from XRD and N_2 adsorption isotherms. TEM images give us the structure of organic and inorganic phases in particles. Alternative black and white lines are observed in the sample before aging as shown in Figure 7A. This supports the XRD results, indicating the presence of micelle rods in the particle even before the aging process. Considering the spherical particle shape observed in SEM images in Figure 2B, the hydrophilic part of the micelle rods, which are already formed in the Ta-$(OEt)_5$−octadecylamine solution, seem to immediately run into the added water drops of spherical particles. After the aging process at 453 K for 7 days, no straight rods were observed, but spots and wormhole-like mesoporous structures were identified in TEM images from various parts. Further aging at 473 K for 24 h was found to have little effect on the pore structure as far as the sample was observed by TEM (Figure 7B). Therefore, it is concluded that homogeneous three-dimensional wormhole-like mesoporous structure is the stable phase for the presently prepared mesoporous Ta_2O_5. The sharpness of the *d*(100) diffraction in XRD patterns of the final product (Figure 3) is attributed to the homogeneous structure.

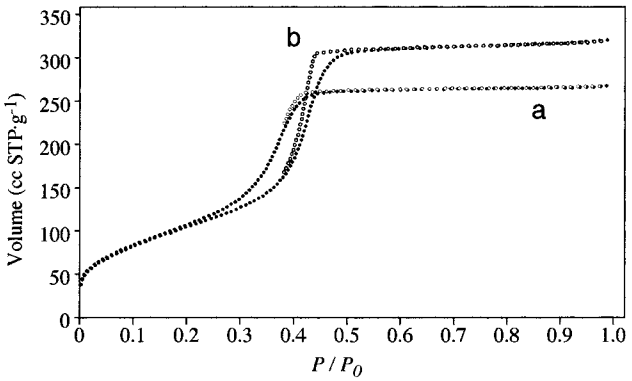

Figure 8. N_2 adsorption and desorption isotherms of mesoporous Ta_2O_5 samples aged at 423 K (a) and at 453 K followed by further aging at 473 K (b).

The transformation of the mesoporous phase during the aging process is also supported by the change of the desorption branch of N_2 adsorption isotherms. Figure 8 compares the N_2 adsorption−desorption isotherms of the samples finally aged at different temperatures: at 423 K for 7 days (a) and at 453 K for 7 days followed by further aging at 473 K for 24 h (b). The shape of the hysteresis loop is known to be reflected by the shape of mesopores,[22] and a change of the desorption branch was observed from Figure 8a to Figure 8b by aging. Type H2 loop (or type IVb isotherm) in Figure 8b indicates the formation of complex and interconnected networks of pores.

(22) Rouquerol, F.; Rouquerol, J.; Sing, K. In *Adsorption by Powderd and Porous Solids*; Academic Press: San Diego, 1999.

Conclusion

The ligand-assisted preparation method of mesoporous Ta_2O_5 was improved, and uniform wormhole-like mesopores were finally formed in amorphous Ta_2O_5 particles. The gradual formation of the pore structure was observed by XRD, TEM, and N_2 adsorption isotherms at different aging temperatures. The precursors of mesopores, micelle rods, were evidenced in particles soon after hydrolysis by TEM. Ordered straight rods were found in the sample after the final aging at 423 K together with the wormhole-like pore structure, and the final aging at either 453 or 473 K resulted in the arrangement of a wormhole-like pore structure.

Acknowledgment. This work was financially supported by Core Research for Evolutional Science and Technology (CREST) of JST (Japan Science and Technology) and partly supported by Research for the Future Program (RFTF), The Japan Society for the Promotion of Science (JSPS) JSPS-RFTF 96R06901, and Grant-in-Aid for International Scientific Research (University-to-University Cooperative Research).

CM000865B